GEOPHYSICS, VOL. 74, NO. 5 (SEPTEMBER-OCTOBER 2009); P. T67–T73, 8 FIGS.
10.1190/1.3157242

Acoustic VTI modeling using high-order finite differences

Stig Hestholm[1]

ABSTRACT

Two second-order wave equations for acoustic vertical transversely isotropic (VTI) media are transformed to six first-order coupled partial differential equations for a more straighforward numerical implementation of the derivatives. The resulting first-order equations have a more natural form for discretization by any finite-difference, pseudospectral, or finite-element method. I discretized the new equations by high-order finite differences and used synthetic seismograms and snapshots for anisotropic and isotropic cases. The relative merits of placing the source deep and close to a free surface are assessed, illustrating advantages of exciting the source inside or outside of a near-surface, thin, isotropic layer. Results show that traveltimes from deep seismic reflectors can remain virtually unaffected when near-surface isotropic layers are included in acoustic VTI media.

INTRODUCTION

Anisotropic behavior of waves in its dynamic and kinematic representation is a vital feature to include in inversion and processing algorithms. The simplest, as well as the most immediately rewarding, anisotropic symmetry is the vertical (or horizontal) transversely isotropic (VTI) modeling scheme. For computational simplicity, this is often implemented in its acoustic version, which yields good results kinematically (important for dip moveout and other processing algorithms) but incorrect results for amplitudes in general elastic/viscoelastic media. This is because VTI conditions do not exist in general acoustic media.

Kinematics (velocities and traveltimes) of P-waves are independent of the S-wave velocity V_{S0} for all practical purposes (Tsvankin and Thomsen, 1994; Alkhalifah, 1998). Therefore, the approximation of setting V_{S0} equal to zero, hence simulating an acoustic medium, has been applied successfully in processing algorithms and wave equations (Alkhalifah, 2000). This acoustic assumption is much more accurate kinematically than weak-anisotropy (Thomsen, 1986) or small-propagation-angle approximations, and it yields more simplified equations.

An unfortunate feature of setting $V_{S0} = 0$ to create the acoustic VTI wave equation is noted in numerical implementations (Alkhalifah, 2000) and identified as SV-waves (Grechka et al., 2004), particularly fast along the vertical and symmetry planes of VTI media. These directions constitute maximum group velocities and zero-phase velocities of SV-waves in acoustic VTI media. The stronger the anisotropy, the higher the SV-wave group velocities along these directions.

However, equality between SV-wave group velocity and P-wave velocity occurs only in the rare case of infinite anellipticity coefficient η (Alkhalifah and Tsvankin, 1995). The SV-wave phase and group velocities are zero everywhere only for isotropic acoustic media and elliptically anisotropic media. In acoustic VTI media, SV-waves can also reflect, transmit, and convert to P-waves at interfaces, interfering with unconverted P-wave arrivals that are usually assumed and used in processing algorithms.

In most cases, SV-wave arrival times and their conversions are distinct from P-wave arrival times. Alkhalifah's (2000) acoustic VTI wave equation provides a practical way of implementing P-wave VTI anisotropy. A transformation of Alkhalifah's (2000) wave equation by Zhang et al. (2003) yields arbitrarily tilted symmetry axes (tilted transversely isotropic [TTI] media) at the cost of additional terms in the wave equations. Zhang et al. (2003) show numerical simulations that agree with previous results for VTI and weak anisotropy. Alkhalifah also derives an acoustic wave equation for orthorhombic symmetry (Alkhalifah, 2003), which is harder to implement numerically because it is a sixth-order partial differential equation (PDE) with respect to time and space.

Alternative second-order PDE formulations (Zhou et al., 2006; Du et al., 2008) are derived from Alkhalifah's (1998) dispersion relation for P-waves in VTI media. Du et al. (2008) show that their formulation gives a linear combination of the physical wavefields of Zhou et al. (2006). Unfortunately, both formulations maintain the unwanted spurious SV-wave as an extra wavefield. They are also second-order PDEs, as in Alkhalifah's (2000) formulation.

Manuscript received by the Editor 2 October 2008; revised manuscript received 10 March 2009; published online 5 August 2009.
[1]CGGVeritas Services, Bergen, Norway E-mail: stig.hestholm@cggveritas.com.

I transform the two second-order wave equations for acoustic VTI media (Alkhalifah, 2000) to three new first-order PDEs with respect to time and space and to one new first-order PDE with respect to space only, suitable for direct numerical discretization by high-order, finite-difference schemes. The three remaining first-order PDEs with respect to time and space are the momentum conservation equations. High-order finite-difference schemes (Fornberg, 1988; Kindelan et al., 1990) are implemented in a staggered grid (Virieux, 1986; Levander, 1988) to approximate the relevant first-order derivatives only. I show synthetic simulations using Euler's (second-order) time-stepping technique and exponential absorbing boundaries (Cerjan et al., 1985) at the bottom and sides of the computational grid to model sources located close to and far away from a free plane surface, inside and outside of a thin isotropic layer.

Finally, I assess the effect on seismic traveltimes when including a near-surface isotropic layer. This is done by simulating three comparable cases: homogeneous VTI, VTI with a near-surface isotropic layer, and homogeneous isotropic.

ACOUSTIC VTI MODELING FORMULATION

Based on the dispersion relation (Alkhalifah, 1998) when setting the vertical shear-wave velocity V_{S0} to zero, Alkhalifah (2000) derives the wave equation for acoustic VTI media in a Cartesian (x,y,z) coordinate system:

$$\frac{\partial^2 P}{\partial t^2} = (1+2\eta)c_{\mathrm{NMO}}^2\left(\frac{\partial^2 P}{\partial x^2}+\frac{\partial^2 P}{\partial y^2}\right)+c_{\mathrm{V}}^2\frac{\partial^2 P}{\partial z^2} - 2\eta c_{\mathrm{NMO}}^2 c_{\mathrm{V}}^2\left(\frac{\partial^4 F}{\partial x^2\partial z^2}+\frac{\partial^4 F}{\partial y^2\partial z^2}\right)+f, \quad (1)$$

where the pressure P is expressed in terms of a wavefield F as

$$P=\frac{\partial^2 F}{\partial t^2}. \quad (2)$$

Here, t is time, and c_{NMO} and c_{V} are the interval NMO and vertical velocities, respectively, where

$$c_{\mathrm{NMO}}(0)\equiv c_{\mathrm{V}}\sqrt{1+2\delta} \quad (3)$$

is the NMO velocity for a horizontal reflector and

$$\eta\equiv 0.5\left(\frac{c_h^2}{c_{\mathrm{NMO}}^2(0)}-1\right)=\frac{\epsilon-\delta}{1+2\delta} \quad (4)$$

is the anellipticity coefficient (Alkhalifah and Tsvankin, 1995; Alkhalifah, 2000), which must be nonnegative for stable solutions of the wave equations (Grechka et al., 2004). The value c_h is the horizontal velocity, and δ and ε are two Thomsen parameters (Thomsen, 1986).

All of these velocities are assumed constant in the derivation of the acoustic VTI equation 1. For most seismic wavelengths, however, the error is small when assuming heterogeneous media, decreasing with increasing signal frequencies. In the following, I assume that the density ρ is locally constant, so the same assumptions are made for the density as for the speeds in equations 1 and 2. The resulting wave equations remain good approximations for seismic wavelengths in heterogeneous media.

With u, v, and w being the three components of the particle velocity, the momentum conservation equations in an acoustic isotropic medium can be written as

$$\frac{\partial P}{\partial x}=-\rho\frac{\partial u}{\partial t}, \quad (5)$$

$$\frac{\partial P}{\partial y}=-\rho\frac{\partial v}{\partial t}, \quad (6)$$

$$\frac{\partial P}{\partial z}=-\rho\frac{\partial w}{\partial t}. \quad (7)$$

The same relationships 5-7 are used to define a convenient (curl-free) particle-velocity field for a VTI medium. Inserting $P = \partial^2 F/\partial t^2$ from equation 2 into equations 5 and 6, we have

$$\frac{\partial^3 F}{\partial x\partial t^2}=-\rho\frac{\partial u}{\partial t}, \quad (8)$$

$$\frac{\partial^3 F}{\partial y\partial t^2}=-\rho\frac{\partial v}{\partial t}. \quad (9)$$

Using the constant-density assumption, we integrate both sides of these equations with respect to t to obtain

$$\frac{\partial^2 F}{\partial x\partial t}=-\rho u+F_1(x,y,z), \quad (10)$$

$$\frac{\partial^2 F}{\partial y\partial t}=-\rho v+F_2(x,y,z). \quad (11)$$

At present, we can set the arbitrary functions $F_1\equiv F_2\equiv 0$ by including them implicitly in the source terms of the final governing wave equations.

Now we differentiate both sides of equations 10 and 11 with respect to x and y, respectively:

$$\frac{\partial^3 F}{\partial x^2\partial t}=-\frac{\partial(\rho u)}{\partial x}, \quad (12)$$

$$\frac{\partial^3 F}{\partial y^2\partial t}=-\frac{\partial(\rho v)}{\partial y}. \quad (13)$$

Then we differentiate both sides of equations 12 and 13 with respect to z and add them together, taking the time derivative outside of the parentheses:

$$\frac{\partial}{\partial t}\left[\frac{\partial^3 F}{\partial x^2\partial z}+\frac{\partial^3 F}{\partial y^2\partial z}\right]=-\frac{\partial}{\partial z}\left(\frac{\partial(\rho u)}{\partial x}+\frac{\partial(\rho v)}{\partial y}\right). \quad (14)$$

Defining

$$\psi=\frac{\partial^3 F}{\partial x^2\partial z}+\frac{\partial^3 F}{\partial y^2\partial z} \quad (15)$$

and

$$\kappa=-\left(\frac{\partial(\rho u)}{\partial x}+\frac{\partial(\rho v)}{\partial y}\right), \quad (16)$$

we obtain

$$\frac{\partial \psi}{\partial t} = \frac{\partial \kappa}{\partial z}. \tag{17}$$

Exchanging order of derivatives, we have from the momentum equations

$$\frac{\partial^2 P}{\partial x^2} = -\frac{\partial}{\partial x}\left[\rho \frac{\partial u}{\partial t}\right] = -\frac{\partial}{\partial t}\left(\frac{\partial(\rho u)}{\partial x}\right), \tag{18}$$

$$\frac{\partial^2 P}{\partial y^2} = -\frac{\partial}{\partial y}\left[\rho \frac{\partial v}{\partial t}\right] = -\frac{\partial}{\partial t}\left(\frac{\partial(\rho v)}{\partial y}\right), \tag{19}$$

and

$$\frac{\partial^2 P}{\partial z^2} = -\frac{\partial}{\partial z}\left[\rho \frac{\partial w}{\partial t}\right] = -\frac{\partial}{\partial t}\left(\frac{\partial(\rho w)}{\partial z}\right). \tag{20}$$

This leads to

$$\frac{\partial^2 P}{\partial x^2} + \frac{\partial^2 P}{\partial y^2} = -\frac{\partial}{\partial t}\left(\frac{\partial(\rho u)}{\partial x} + \frac{\partial(\rho v)}{\partial y}\right) = \frac{\partial \kappa}{\partial t}, \tag{21}$$

which, together with equations 15 and 20, results in the following form of Alkhalifah's (2000) acoustic VTI wave equation 1:

$$\frac{\partial^2 P}{\partial t^2} = (1 + 2\eta) c_{\mathrm{NMO}}^2 \frac{\partial \kappa}{\partial t} - c_{\mathrm{V}}^2 \frac{\partial}{\partial t}\left(\frac{\partial(\rho w)}{\partial z}\right) - 2\eta c_{\mathrm{NMO}}^2 c_{\mathrm{V}}^2 \frac{\partial \psi}{\partial z} + f. \tag{22}$$

I define a new field variable ζ such that

$$\frac{\partial \zeta}{\partial t} = \psi. \tag{23}$$

Inserting this into the second-to-last term of equation 22 and exchanging the order of the derivatives leads to

$$\frac{\partial^2 P}{\partial t^2} = (1 + 2\eta) c_{\mathrm{NMO}}^2 \frac{\partial \kappa}{\partial t} - c_{\mathrm{V}}^2 \frac{\partial^2(\rho w)}{\partial t \partial z} - 2\eta c_{\mathrm{NMO}}^2 c_{\mathrm{V}}^2 \frac{\partial^2 \zeta}{\partial t \partial z} + f. \tag{24}$$

Finally, integrating everywhere with respect to t yields three new governing first-order PDEs in acoustic VTI media:

$$\frac{\partial P}{\partial t} = (1 + 2\eta) c_{\mathrm{NMO}}^2 \kappa - c_{\mathrm{V}}^2 \frac{\partial(\rho w)}{\partial z} - 2\eta c_{\mathrm{NMO}}^2 c_{\mathrm{V}}^2 \frac{\partial \zeta}{\partial z} + G, \tag{25}$$

$$\frac{\partial \psi}{\partial t} = \frac{\partial \kappa}{\partial z}, \tag{26}$$

$$\frac{\partial \zeta}{\partial t} = \psi, \tag{27}$$

where definition 16 is added and definition 15 is assumed but not used in the numerical implementation.

The value G is the volume force consisting of the time-integrated f plus a time-independent source term D:

$$G = \int_{-\infty}^{\infty} f dt + D(x,y,z), \tag{28}$$

where $D(x,y,z)$ can be set to zero for any selected source function f. A similar choice of source function is made by choosing F_1 and F_2 equal to zero in equations 10 and 11. The momentum conservation equations 5–7 constitute the remaining three first-order PDEs for wavefield modeling in an acoustic VTI medium.

NUMERICAL DISCRETIZATION

The advantage of this new wave-equation formulation 25-27 is its form of first-order PDEs only, which makes high-order finite-difference discretization on a numerical grid straightforward and natural. It also smooths application of alternative methods of numerical discretization, such as finite elements and pseudospectral methods. By taking advantage of the simple form of the Euler (leapfrog) time-stepping method, only one value per time step of every field variable must be stored.

Seven field variables must be updated at every time step: ρu, ρv, ρw, P, κ, ψ, and ζ. The additional full-grid variables needed in the wavefield model are the input parameters c_{V} and c_{NMO} (the vertical and NMO velocities), the anellipticity parameter η, the volume force G, and optionally the density ρ — only if the particle velocities are required. These are the same input parameters necessary in Alkhalifah's (2000) second-order PDE formulation. The field variables in my formulation obviously are different, with the exception of the pressure P.

When the particle velocities are calculated, the total number of field variables necessary in my formulation and in Alkhalifah's (2000) formulation amount to the same; so the total memory requirements are alike in the two formulations. Apart from input material parameters, Alkhalifah's (2000) second-order PDE formulation (equations 1 and 2) requires two values each of P and F at each grid point, in addition to possible particle-velocity components (if required) in a numerical implementation. In total, this is seven wavefields to be maintained, the same number as in my formulation.

To minimize a strong SV-wave emanating from the source when applying the acoustic VTI wave equations (Alkhalifah, 2000; Grechka et al., 2004) and to increase long-term stability of simulations, the source is often placed in a thin, isotropic layer at the top of the medium, close to the free surface. For this reason, I implement isotropic free-surface boundary conditions for particle velocities (Hestholm and Ruud, 2002) and apply them in numerical simulations on top of a thin, isotropic, upper medium layer. Cerjan et al.'s (1985) exponential damping method is used for wavefield absorption along the bottom and sides of the grid.

The staggered 3D grid I use (Figure 1) displays the positions at which the field variables ρu, ρv, ρw, P, κ, ψ, and ζ are defined. It also shows the input parameters c_{V}, c_{NMO}, η, ρ, and G. By this definition, every term in the new governing equations 25–27 and 5–7 is defined at a single point in the grid for each equation, a necessary condition for long-term numerical stability in any finite-difference discretization. By using the free-surface boundary conditions (Hestholm and Ruud, 2002) and the grid of Figure 1, P can remain undefined at the free surface because the particle velocities u, v, and w (or, alternatively, ρu, ρv, and ρw) are defined there from known

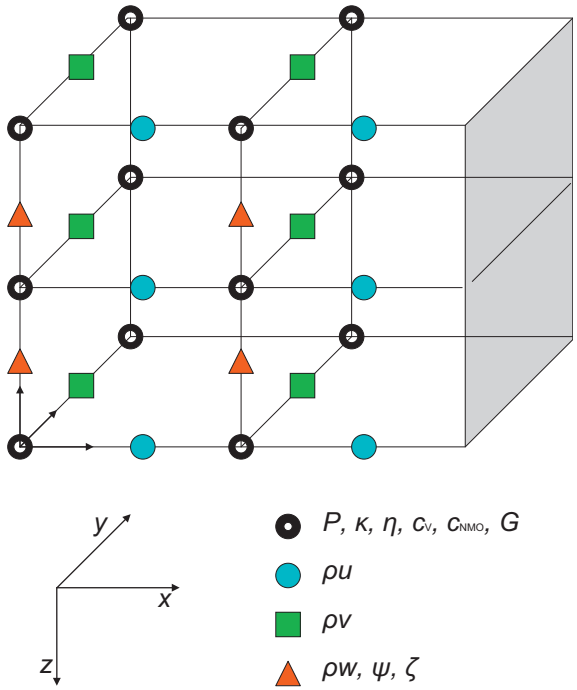

Figure 1. Grid for finite-difference discretization of first-order acoustic VTI wave equations. The designations in the grid of each wavefield and model parameter are shown by symbols.

wavefields in the interior of the medium. The default output field is P, and u, v, and w can be output optionally if ρ is given as input data.

Eighth-order finite-difference methods for a staggered grid (Holberg, 1987; Fornberg, 1988; Kindelan et al., 1990) are used in simulations with gradually decreasing orders when approaching all medium boundaries, including the free surface. Eighth-order, then sixth-, fourth-, and finally second-order staggered central finite differences (Fornberg, 1988), are used when moving from the interior medium toward a boundary. Just as for the second-order wave equation 1 of Alkhalifah (2000), I conjecture the same stability criterion to be valid for the new first-order wave equations 25–27 as for the isotropic case, i.e., the Courant criterion (Courant et al., 1928).

SIMULATION EXAMPLES

Figures 2 and 3 show corresponding simulations for an acoustic anisotropic VTI medium and for an isotropic medium. In each example, a spatially Gaussian distributed source is placed at a 1.25-km depth at $x = 1.7$ km and $y = 0.5$ km of the model, which consists of $680 \times 280 \times 580$ points in the x-, y-, and z-(vertical) directions, respectively, and has a uniform grid length of 5 m. This constitutes a domain of $3.4 \times 1.4 \times 2.9$ km, including 40 grid points of absorbing layers of 200 m thickness along the sides and bottom of the domain. The snapshots of the pressure are taken along the xz-plane at the middle of the y-direction ($y = 0.7$ km), so the snapshot plane is 0.2 km behind the source point.

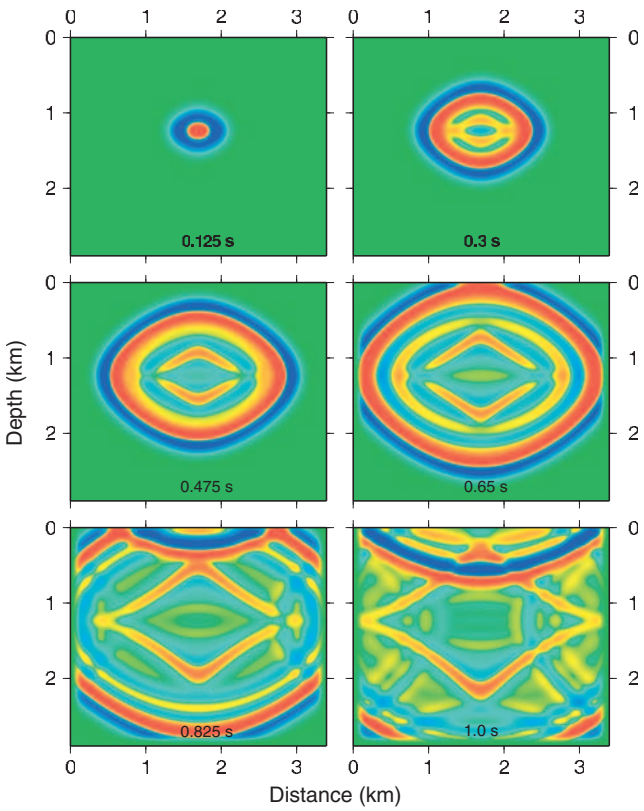

Figure 2. Snapshots of P from a Gaussian distributed source at $x = 1.7$ km and $y = 0.5$ km at a 1.25-km depth. The snapshots are taken along an xz-plane at $y = 0.7$ km of a homogeneous acoustic VTI medium with $\eta = 0.4$.

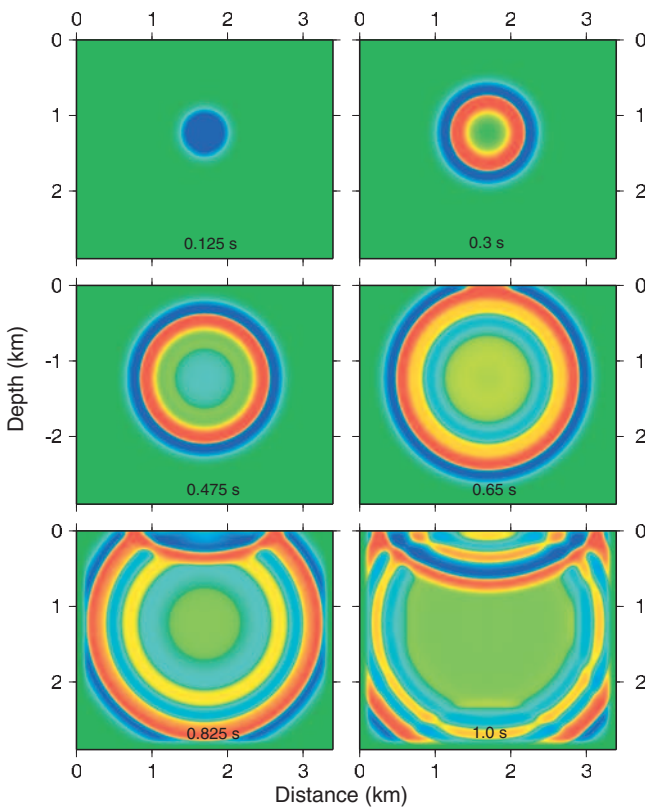

Figure 3. Snapshots of P from a Gaussian distributed source (as in Figure 2) at $x = 1.7$ km and $y = 0.5$ km at 1.25-km depth. The snapshots are taken along an xz-plane at $y = 0.7$ km of a homogeneous acoustic isotropic medium.

The vertical c_V and NMO P-wavespeed c_{NMO}, as well as the isotropic P-wavespeed, are 2 km/s for homogeneous media, and the density is uniformly 2000 kg/m^3. The anellipticity coeffient η is 0.4 in the VTI example (Figure 2). The vertical wavespeed for the VTI medium is the same as the wavespeed for the isotropic example. The VTI horizontal speed resulting from the applied value for η is significantly larger than the vertical one, as can be confirmed. The source's central frequency in time is 30 Hz with a Ricker profile, which represents an exploration experiment quite well. There is a big difference in the appearance of the excited waves in the two cases. The additional SV-wave that occurs at the source following the P-wave in the VTI case (Alkhalifah, 2000; Grechka et al., 2004) clearly occurs as a diamond-shaped wave pattern with maximum wavespeeds along the VTI axis and the isotropy plane.

Figure 4 shows snapshots of P for a homogeneous VTI medium; Figure 5 is for the same medium with an added 0.5-km-deep, near-surface isotropic layer. In both cases, $\eta = 0.5$, the model size and dimensions are as before, and a Gaussian spatially distributed source with a Ricker time profile with 30-Hz central frequency is located close to the middle position of the near-surface layer, i.e., at a depth of 0.25 km, $x = 1.7$ km, and $y = 0.5$ km.

As expected from previous experiments (Alkhalifah, 2000; Zhang et al., 2003), positioning the P-source inside the isotropic layer eliminates exciting SV-waves from the source — the opposite of what happens in the homogeneous VTI experiment (Figure 4). The clear, diamond-shaped SV-wave excites out of the source point, leading to possible problems for subsequently applied processing algorithms that assume only primary P-wave events. Such an assumption is of course a significant limitation, even without the spurious SV-wave, because of internal and free-surface multiples and surface waves. Therefore, the extra SV-wave does not simplify the situation. Hence, including an isotropic near-surface layer with physical properties similar to those of the remaining medium, which includes the source, seems a reasonable improvement to avoid unwanted SV-waves excited in VTI media.

Next is an approximate assessment as to which degree the isotropic near-surface layer affects traveltimes in anisotropic media. Figure 6 is a shot record of seismograms for a VTI medium of a uniform $\eta \equiv 0.5$, with a Gaussian distributed source of 30-Hz central frequency released at a depth of 0.25 km at $x = 1.7$ km and $y = 0.5$ km. The medium has a horizontal reflector at a 1-km depthwith speeds and densities of $v_{P1} = 2000$ m/s, $\rho_1 = 2000$ kg/m^3, $v_{P2} = 2500$ m/s, and $\rho_2 = 2500$ kg/m^3, from top to bottom. The given P-velocities are for c_V and c_{NMO}, i.e., for the vertical velocity and the NMO velocity for a horizontal reflector. The receivers are located along the x-direction at $y = 0.7$ km from $x = 1.25$ to $x = 2.15$ km at 5-m spacing and 10-m depth. Figure 7 is a seismogram for the same model, source, and receiver configuration, with an added near-surface isotropic layer of 0.5-km depth.

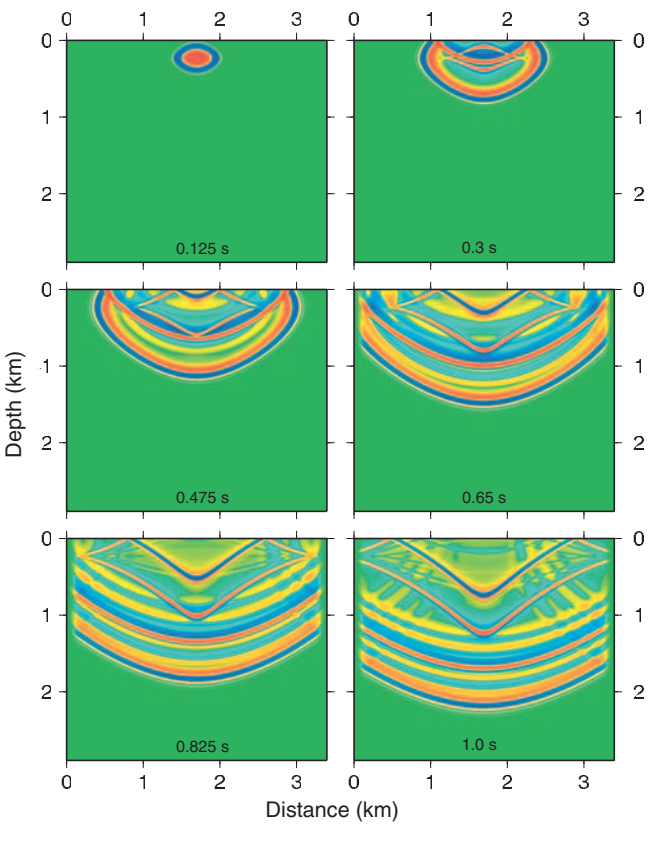

Figure 4. Snapshots of P from a Gaussian distributed source at $x = 1.7$ km and $y = 0.5$ km at 0.25-km depth. The snapshots are taken along an xz-plane at $y = 0.7$ km of a homogeneous acoustic VTI medium with $\eta = 0.5$.

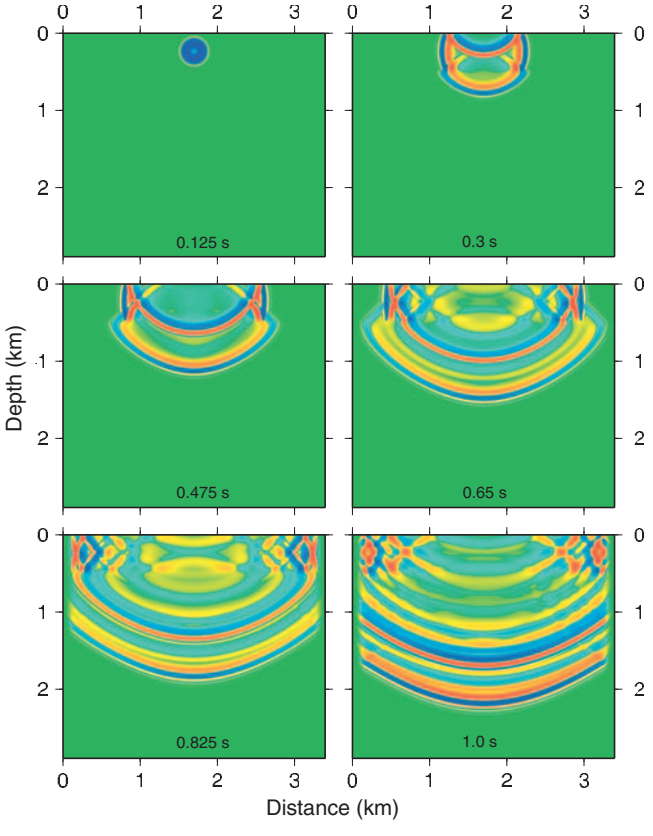

Figure 5. Snapshots of P from a Gaussian distributed source (as in Figure 4) at $x = 1.7$ km and $y = 0.5$ km at 0.25-km depth. The snapshots are taken along an xz-plane at $y = 0.7$ km. The acoustic VTI medium has $\eta = 0.5$ and a near-surface acoustic isotropic layer of 0.5-km depth. Compare with Figure 4.

Apart from slower arrival times of the initial P-wave in the latter model, which is from the near-surface isotropic layer, the strong SV-wave arrival in the pure VTI medium of Figure 6 is avoided in Figure 7. However, three distinct extra arrivals are identified because of the near-surface isotropic layer in Figure 7: (1) the long-wavelength arrival starting around 0.39 s (the first reflection from the boundary between the isotropy and anisotropy layer), (2) the arrival starting at around 0.62 s (the anisotropic-layer reflection of the surface ghost), and (3) the arrival starting around 0.78 s (the first multiple of the anisotropic-layer reflection). The wave marked S in Figure 6 can be confused with a reflection but is in fact a P-wave along the free surface caused by the unwanted SV-wave from the source. An interesting and important feature is that the first reflection from the boundary at 1 km, which occurs at around 0.88 s, has arrival times that are practically indistinguishable from each other in the two simulations.

Extra, unwanted arrivals occur from the near-surface isotropic-layer boundary in Figure 7. A more smooth transition could be used to minimize these; alternatively, pure VTI media could be used in simulations. After all, slow SV-waves of the VTI example are easier to suppress during processing than the extra P-reflections. However, the SV-waves generated in homogeneous VTI examples convert to P-waves at interfaces, leading to problems for algorithm processing. The near-surface isotropic layer used in Figure 7 is deeper than is strictly necessary to avoid unwanted SV-waves, so reflections from the bottom of this layer may occur earlier. The contrast between the layers is also particularly strong with $\eta = 0.5$.

In real life, near-surface isotropic layers usually exist (in marine experiments they always do), and they usually do not have a sharp discontinuity with the lower VTI medium. Hence, they do not cause unwanted reflections as here. Even with the near-surface isotropic layer being relatively deep as in this example, the arrival times of first reflections from the deeper medium-layer boundary are very similar for the two model alternatives. Traveltime differences are relatively smaller with reflector depth. At any rate, traveltime is the only feature we can hope to model accurately using acoustics only.

The corresponding experiment for a completely isotropic medium is included in Figure 8 for reference. With the present reflector depth and small aperture, there is minimal difference in traveltime from the reflector at a 1-km depth, with and without VTI included, although a difference can be noted (the arrival starting around 0.88 s in Figures 6 and 8). For the direct wave, the relative offset is large enough to see the strong effect of traveltimes on arrivals.

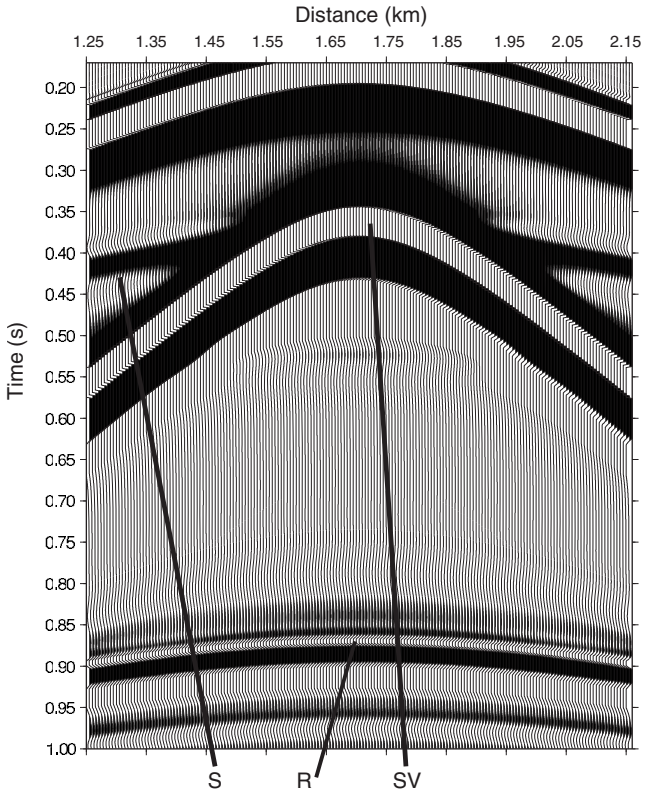

Figure 6. Pressure seismograms of a simulation of a Gaussian source at 0.25-km depth, $x = 1.7$ km, and $y = 0.5$ km in a VTI medium of $\eta = 0.5$. A plane reflector is at 1-km depth with $v_{P1} = 2000$ m/s, $\rho_1 = 2000$ kg/m^3, $v_{P2} = 2500$ m/s, and $\rho_2 = 2500$ kg/m^3 in the upper layer and lower half-spaces, respectively. The P-velocities are for c_V and c_{NMO} (see text). The receivers are 10 m deep at $y = 0.7$ km from $x = 1.25$ to $x = 2.15$ km at 5-m spacing. Energy R is from the plane reflector. Energy S is the P-wave at the surface caused by the secondary SV-wave from the source, which also is marked. Compare with Figure 7.

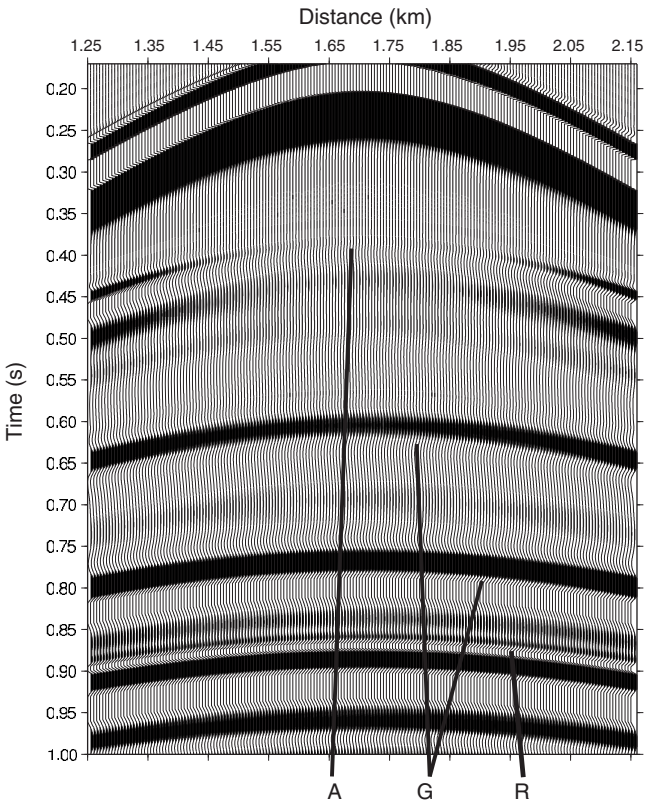

Figure 7. Pressure seismograms for the same source, source location, and medium of Figure 6 with a 0.5-km-deep near-surface isotropic layer added. The receivers are 10 m deep at $y = 0.7$ km from $x = 1.25$ to $x = 2.15$ km at 5-m spacing. Energy A is the first reflection from the bottom of the isotropic layer; energy G is the isotropic layer reflection of the surface ghost and the first multiple of the isotropic layer reflection. Compare with Figure 6, where R is from the plane layer reflector at a 1-km depth, as it is here.

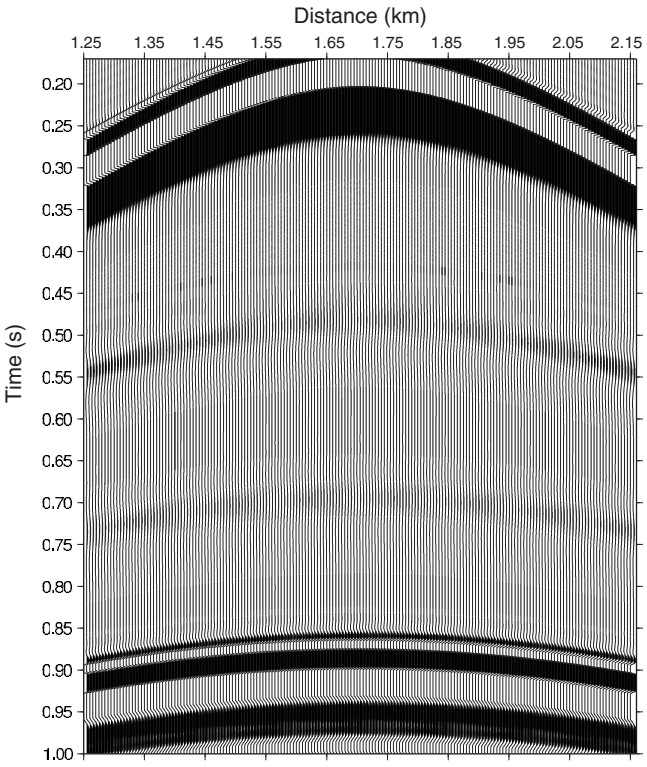

Figure 8. Pressure seismograms for the source and model in Figure 6 but for an isotropic medium. The receivers are 10 m deep at $y = 0.7$ km from $x = 1.25$ to $x = 2.15$ km at 5-m spacing. Compare with Figures 6 and 7.

CONCLUSIONS

A previous second-order acoustic VTI wave equation is transformed to six coupled first-order PDEs to facilitate easy numerical discretization by methods other than second-order finite differences. Such methods are finite elements, pseudospectral, and higher-order finite differences. Discretizations of new wave equations are done by eighth-order finite differences, with a gradual decrease of finite-difference order near numerical grid boundaries. I display the exact definition of all field variables and material parameters in a staggered grid. This discretization is used to define all terms in the equations consistently at one grid point only for each wave equation, a condition generally necessary for acceptable accuracy and long-term numerical stability.

I have simulated known features of P-wave sources excited in acoustic VTI media, including an unwanted SV-wave that emanates from the source later than the P-wave. This fact often makes it possible to attenuate the SV-wave in processing algorithms. At any rate, it may convert to P-waves, which will affect processing results negatively. One way to eliminate the additional SV-wave is to include the source in a near-surface isotropic layer, which usually exists in nature without constituting sharp interfaces, hence avoiding seismic interface reflections. Whether or not such a layer is used, one or two grid points at the free surface may be made isotropic, which proves constructive for long-term stability of simulations. At the free-plane surface, I implement free-surface topography boundary conditions for the particle velocities. Using some form of acoustic VTI equations is a practical approach in full-waveform inversion because of the computational efficiency. Applying fully general VTI or TTI elastic wave equations is still quite expensive in reverse time migration.

ACKNOWLEDGMENTS

I acknowledge Vladimir Grechka for useful comments, Jim Clippard for motivating the research, and Tariq Alkhalifah and two anonymous reviewers for improving this paper. I also acknowledge Shell International E&P Inc. for permission to publish an extended abstract and CGGVeritas Services for permission to publish the present work. I acknowledge support from the Norwegian Research Council through a grant of computing time.

REFERENCES

Alkhalifah, T., 1998, Acoustic approximations for processing in transversely isotropic media: Geophysics, **63**, 623–631.

———, 2000, An acoustic wave equation for anisotropic media: Geophysics, **65**, 1239–1250.

———, 2003, An acoustic wave equation for orthorhombic anisotropy: Geophysics, **68**, 1169–1172.

Alkhalifah, T., and I. Tsvankin, 1995, Velocity analysis for transversely isotropic media: Geophysics, **60**, 1550–1566.

Cerjan, C., D. Kosloff, R. Kosloff, and M. Reshef, 1985, A nonreflecting boundary condition for discrete acoustic and elastic wave equations: Geophysics, **50**, 705–708.

Courant, R., K. Friedrichs, and H. Lewy, 1928, Uber die partiellen Differenzengleichungen der mathematischen Physik: Mathematische Annualen, **100**, 32–74.

Du, X., R. P. Fletcher, and P. J. Fowler, 2008, A new pseudo-acoustic wave equation for VTI media: 70th Annual Technical Conference & Exhibition, EAGE, Extended Abstracts, H033.

Fornberg, B., 1988, Generation of finite difference formulas on arbitrary spaced grids: Mathematics of Computation, **51**, 699–706.

Grechka, V., L. Zhang, and J. W. Rector III, 2004, Shear waves in acoustic anisotropic media: Geophysics, **69**, 576–582.

Hestholm, S. O., and B. O. Ruud, 2002, 3D free-boundary conditions for coordinate-transform finite-difference seismic modeling: Geophysical Prospecting, **50**, 463–474.

Holberg, O., 1987, Computational aspects of the choice of operator and sampling interval of numerical differentiation in large-scale simulation of wave phenomena: Geophysical Prospecting, **35**, 629–655.

Kindelan, M., A. Kamel, and P. Sguazzero, 1990, On the construction and efficiency of staggered numerical differentiators for the wave equation: Geophysics, **55**, 107–110.

Levander, A. R., 1988, Fourth-order finite-difference P-SV seismograms: Geophysics, **53**, 1425–1436.

Thomsen, L., 1986, Weak elastic anisotropy: Geophysics, **51**, 1954–1966.

Tsvankin, I., and L. Thomsen, 1994, Nonhyperbolic reflection moveout in anisotropic media: Geophysics, **59**, 1290–1304.

Virieux, J., 1986, P-SV wave propagation in heterogeneous media: Velocity-stress finite-difference method: Geophysics, **51**, 889–901.

Zhang, L., J. W. Rector III, and G. M. Hoversten, 2003, An acoustic wave equation for modeling in tilted TI media: 73rd Annual International Meeting, SEG, Expanded Abstracts, 153–156.

Zhou, H., G. Zhang, and R. Bloor, 2006, An anisotropic acoustic wave equation for VTI media: 68th Annual Technical Conference & Exhibition, EAGE, Extended Abstracts, H033.